Reaction dynamics studied via positron and electron spectroscopy

R. Krieg, E. Bożek,* U. Gollerthan, E. Kankeleit, G. Klotz-Engmann, M. Krämer, U. Meyer, H. Oeschler, and P. Senger†
Institut für Kernphysik, Technische Hochschule Darmstadt, Federal Republic of Germany
(Received 31 December 1985)

The dynamics of collisions between very heavy ions have been studied via their influence on the positron and δ-electron spectra using the Tori spectrometer, a new magnetic transport system which is able to measure positrons and electrons simultaneously. The spectra obtained in coincidence with elastic scattering agree well at all measured energies with theory based on Rutherford trajectories, while a steeper slope is observed in spectra measured in coincidence with dissipative collisions. These spectra can only be described by calculations taking into account a nuclear contact time of up to 2×10^{-21} s in the collision process.

I. INTRODUCTION

In heavy ion collisions the two nuclei form, for a short time, a quasiatom with rapidly changing Coulomb potential.[1] This induces the emission of electrons from all levels—including those from the Dirac sea creating thereby "atomic" positrons. The collision dynamics between very heavy ions can be studied by the spectroscopy of these particles as their spectral distributions reflect the Fourier frequencies of the time evolution of the collision process.[2] If the Rutherford trajectories are perturbed by nuclear forces, the Fourier frequency spectrum and hence the spectra of δ electrons and positrons will be altered.[2] Experiments have been performed to study the dynamics of elastic and dissipative heavy ion collisions by the spectroscopy of δ electrons and positrons.[3]

To get an understanding of the dynamically induced positron and electron creation we outline here the main aspects of this process within the framework of first order perturbation theory.[2] For direct excitations of an electron-positron pair the transition amplitude reads

$$a_{if}=-\int_{-\infty}^{\infty}dt\langle f\,|\,\partial/\partial t\,|\,i\rangle \times\exp\left[i\int_{-\infty}^{t}dt'(E_f-E_i)/\hbar\right] \quad (1)$$

with E_f and E_i the total energy of initial and final state, respectively. As the perturbation is caused by the time evolution of the Coulomb potential, the amplitude can be written as

$$a_{if}\simeq[(\rho R^2)_i(\rho R^2)_f]^{1/2} \times(1/\Delta E)\int_{-\infty}^{\infty}dt\,\dot{R}/R\exp\left[\int_{-\infty}^{t}dt'\Delta E/\hbar\right] \quad (2)$$

with $\rho=\rho(0)$ the initial and final density of e^+ and e^- at the origin, R the distance between the nuclei and $\Delta E=E_f-E_i$ the mean transferred energy. Thereby rotational coupling is neglected and only the monopole term of the time-dependent Coulomb potential of the quasiatom is taken into account.

For elastic collisions the time between the extrema of the $\dot{R}/R$ curve (Fig. 1, dashed line) can be defined as the collision time $2\hat{t}$. Using the approximations introduced in Ref. 2,

$$\dot{R}/R\simeq t/(t^2+\hat{t}^2) \quad (3)$$

with

$$2\hat{t}\simeq(2a/v)(\epsilon+1.6+0.5/\epsilon) \quad (4)$$

(ϵ is the eccentricity, $2a$ the minimum distance of closest approach, and v the projectile velocity), the energy-differential production probability is obtained. For positrons it reads

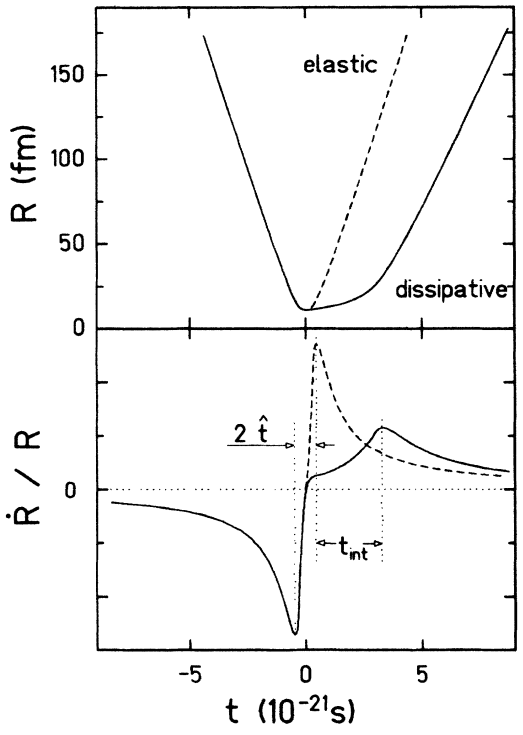

FIG. 1. Time dependence of R (distance between the two nuclei) and $\dot{R}/R$ ($\dot{R}$ relative velocity).

$$dP/dE_{e+} \simeq h(E_{e+},\hat{t})/(E_{e+}+2m_0c^2)^2 \times \exp[-2\hat{t}(E_{e+}+2m_0c^2)/\hbar] , \quad (5)$$

where E_{e+} is the kinetic energy of the positron and the weak dependence of ΔE on the kinetic energy of the electron is neglected. The function $h(E_{e+},\hat{t})$ originates from the square root term in Eq. (2) and is responsible for the decrease of the positron intensity towards low energies closely related to the Fermi function in the beta decay. For electrons $h(E_{e-},\hat{t})$ is nearly energy independent and one obtains

$$dP/dE_{e-} \simeq (E_{e-}+E_b)^{-2}\exp[-2\hat{t}(E_{e-}+E_b)/\hbar] \quad (6)$$

with E_{e-} the kinetic energy of the electron and E_b an effective binding energy. Hence the spectra of the emitted electrons as well as the high-energetic tail of the positron spectra are nearly exponential with $\hat{t}$ defining the slope (Fig. 2, dashed line).

In contrast to elastic scattering, the motion of the nuclei in dissipative collisions is damped due to nuclear friction, i.e., the collision time is increased by t_{int} (Fig. 1, full line). This causes a phase shift $\Delta\phi = \Delta E t_{int}/\hbar$ between ingoing and outgoing production amplitudes (Fig. 3) which for a fixed transferred energy leads to oscillations in the production probability as a function of t_{int}. Vice versa, for a fixed nuclear contact time one obtains oscillations in dP/dE where the period is given by h/t_{int} (Fig. 2: examples are the dashed-dotted and dotted lines). A distribution of interaction times smears out these structures and yields a steeper decline of the spectrum in the energy range around 1 MeV (Fig. 2: full line).

It should be stressed that this model describes direct excitations with well defined electronic states. Dominantly, multistep processes occur and the δ electrons are emitted from various quasiatomic levels. These effects are taken into account by coupled-channels calculations.[4] Nevertheless, our simple model can be used to extract information about the collision dynamics from the data as it reproduces very well the shape of the spectra. However, it does not predict absolute intensities.

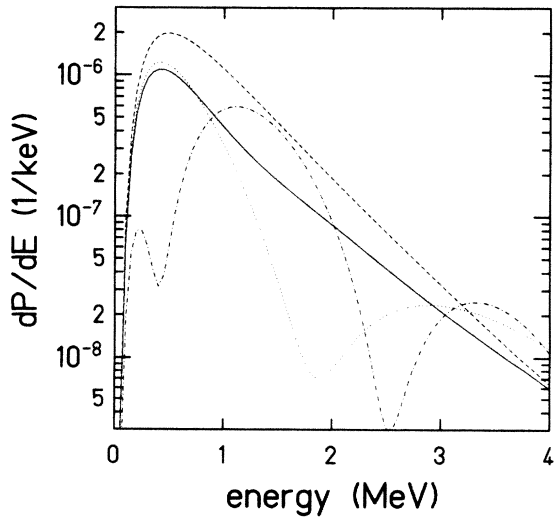

FIG. 2. Calculated positron spectra for elastic and dissipative collisions (see text).

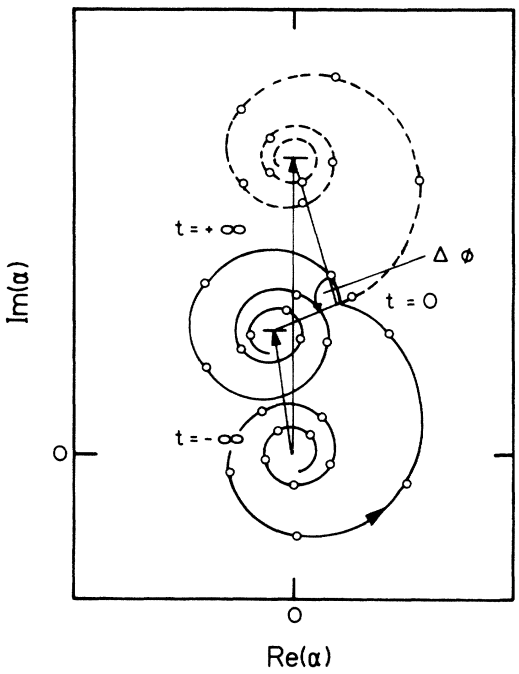

FIG. 3. The transition amplitude as a function of time for elastic (dashed line) and dissipative (solid line) collisions showing the phase shift $\Delta\phi$.

We studied time delay effects in the collision system U + U at beam energies from the Coulomb barrier (5.9 MeV/nucleon) up to 10 MeV/nucleon. Comparing the measured positron and electron spectra with theoretical calculations, we test various reaction models (Sec. IV). The nuclear contact time appears as an essential parameter in this comparison.

A main difficulty in measuring positrons is caused by their very low production probability. Additionally, they are embedded in a background of electrons occuring about 10^4 times more frequently. Our new experimental setup, the Tori spectrometer,[5] combines well a large efficiency for positrons with a high suppression of electrons (Sec. II). A crucial problem in studying positrons from atomic processes is the contribution of positrons originating from pair-converted transitions of excited nuclear levels. The measured spectra have to be corrected for these positrons before comparing with theory. The correction procedure is described in Sec. III B.

In the discussion (Sec. IV) we first compare one measured spectrum with predictions based on three models describing dissipative collisions. For simplicity, the electronic excitations are calculated using the perturbation theory discussed above. Then one friction model is chosen for the comparison with the data taken at the different incident energies. For this detailed analysis the atomic processes are treated by the coupled-channels calculations including also electron screening effects.[4] One

part of this work is devoted to experiments with restricted impact parameter regions. As one possibility, subgroups of dissipative collisions are selected in the hope they represent a small variation of nuclear interaction times (Sec. IV B 2).

II. EXPERIMENT

The systematic study of U + U collisions is the first experimental series carried out with a new type of magnetic transport system, the so-called Tori spectrometer.[5] It is able to measure positrons and electrons simultaneously without influencing each other. It consists essentially of two quarter toroids forming an "S-shaped solenoid." A detailed description of the apparatus is given in Ref. 5. Here we only explain the essential features of the instrument.

The field of the Tori spectrometer has a $1/R$ dependence with R the distance from the center of a toroid. While in homogeneous magnetic fields charged particles spiral around the field lines, the particles experience in the Tori spectrometer different magnetic field strengths during one turn which leads to a drift perpendicular to the field lines and to the field gradient in opposite directions according to the sign of their charges.

The main components of the apparatus are depicted in Fig. 4. In the first quarter toroid, positrons and electrons drift in opposite directions on their way to the middle plane where they are spatially completely separated. Here the electrons are absorbed by a semicircular diaphragm above which a detector arrangement consisting of three Si(Li) diodes is installed (see Ref. 5). Only a few of the electrons scattered at the diaphragm or on the walls of the tube can reach the second quarter toroid. Measurements with beta and conversion electron sources show that the suppression is nearly 10^4:1.

Positrons pass unhindered through the middle plane and drift back to the central line in the second quarter where they reach a Si(Li) diode with a diameter of 5 cm and a depth of 5 mm. The advantage of this setup is a high transmission of 80% for particles with energies up to 650 keV and a slow decrease of transmission towards higher energies.

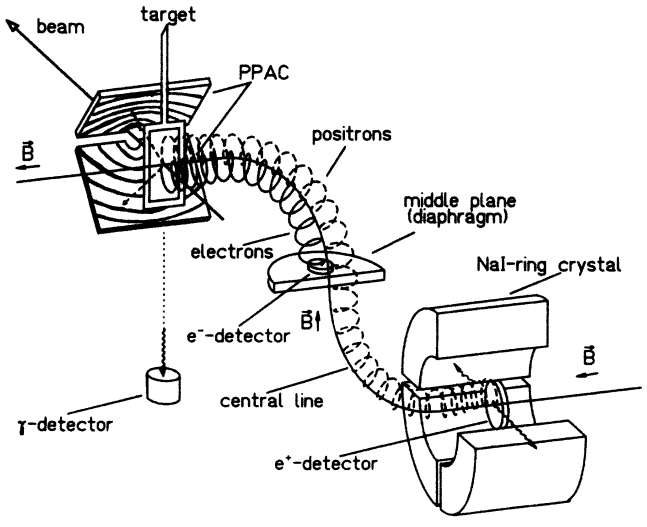

FIG. 4. The Tori spectrometer and its detection devices.

In order to discriminate the positrons from scattered electrons, their annihilation radiation is identified by a four-sector NaI-ring crystal. Various conditions concerning the numbers and the energies of the required NaI signals are used:[5] The strongest one requires two photopeak signals of 511 keV in opposite NaI segments, but then only 5% of the emitted positrons are accepted. In the weakest one a single γ ray within the energy range of the Compton continuum or the photopeak in one of the NaI segments is demanded (efficiency 40%). The analysis was carried out under the condition of a coincidence between a full-energy signal in one crystal and a Compton-continuum or photopeak signal in the opposite one yielding an efficiency of 15% in the maximum. It has been verified that summing of the positron energy signal with Compton-scattered annihilation radiation in the Si(Li) diode can be neglected.[5]

The scattered heavy ions are detected by a pair of position-sensitive parallel-plate avalanche counters (PPAC) covering the angular range from 18 to 70 degrees. The anode plane is divided into conic-sectioned copper stripes corresponding to $\Delta\theta = 2°$ which are connected by 2 ns delay lines. By reading out both ends of the delay-line chain, double events in one counter can be detected and the fission of one or both partners can thus be observed. Additionally, scattered heavy ions can be distinguished from fission fragments by the energy-loss signal. The angular correlation allows separation of elastic scattering, inelastic reactions and sequential fission as well.

In order to detect γ rays originating from nuclear reactions, a 7.5×7.5 cm NaI crystal is mounted at an adjustable distance of 30 to 80 cm from the target. The counting rate and the spectral distribution of the γ rays allow an estimation of the contribution of positrons created by internal pair conversion as described in Sec. III B.

The experiments were performed with the UNILAC accelerator at GSI delivering ^{238}U beams of about 60 nA (charge state 40+) at energies of 5.9, 7.5, 8.4, and 10.0 MeV/nucleon. The diameter of the beam spot at the target, defined by a slit system, was 3 mm.

The targets consisted of 500 μg/cm^2 ^{238}U sandwiched between ^{12}C foils of 15 and 35 μg/cm^2. Natural Tm targets of 500 μg/cm^2 and ^{108}Pd targets of 1 mg/cm^2 were used.

The data were collected with a PDP11/45 linked to an IBM 308X for recording up to 10^3 events/s. With the beam current indicated above, about one to five positrons per second were observed.

III. DATA ANALYSIS

A. Data analysis and correction for detector response

The energy spectra of positrons, electrons, and gamma rays are classified according to the collision process they are produced in. The classification into elastic scattering at various angles or dissipative collisions followed by sequential fission with three- and four-body exit channels

at various Q values is done by kinematical windows in the θ_1-θ_2 plane (θ_1 and θ_2 are the polar angles of the scattered particles), by the number of detected fragments and by the ΔE signal in the PPAC distinguishing fission fragments from scattered U-like nuclei. To obtain the production probability for the different classes the spectra are divided by the particle counting rate obtained under the same condition. Prompt events are selected in the usual way. As an example, Fig. 5(a) shows the time difference between gamma-ray and particle signals. The prompt peak has a full width at half maximum (FWHM) of 2.5 ns (corrected for the time of flight of the reaction products). Chance coincidences are obtained from the number of coincidences in neighboring micropulses. Gamma rays induced by neutrons are separated due to the flight time. They appear to the right side of the prompt peak.

Figure 5(b) shows a time spectrum between one NaI segment and the positron Si(Li) diode. The FWHM is 12 ns and the background from chance coincidences is negligible ($<1\%$).

Figure 6 shows a typical raw spectrum of positrons (full-line histogram). An iterative matrix-multiplication algorithm[6] was used to unfold the raw spectra with the response function of the detector as determined with calibration sources (dotted curve in Fig. 6). The energy-dependent efficiency of the detectors was corrected for as well.

B. Positrons from nuclear pair conversion

The determination of the so-called nuclear positrons is one of the main problems in positron spectroscopy. One possibility is to calculate this contribution by converting the measured gamma spectrum $dN(E_\gamma)/dE_\gamma$ into a spectrum of "nuclear" positrons. Each γ transition has to be converted into a positron spectrum according to

$$dN(E_{e+})=dN(E_\gamma)d\beta/dE_{e+}(E_\gamma,E_{e+},Z,M\lambda)\ , \qquad (7)$$

where $d\beta/dE_{e+}$ is the pair conversion coefficient depending on the γ energy E_γ, on the nuclear charge Z, and the multipolarity of the transition $M\lambda$. While in elastic scattering the charge of the nuclei remains unchanged, in dissipative collisions followed by sequential fission it is sufficient to base the calculations on half of the uranium's charge, because the coefficients depend nearly linearly on Z. The multipolarity of the transitions $M\lambda$ is unknown.

Figure 7 shows typical gamma spectra from elastic and dissipative U + U collisions at different beam energies. In order to investigate the multipolarity, experiments with uranium beams on lighter target nuclei were carried out. In earlier experiments[7] with a broad variety of projectile-target combinations, it turned out that the atomic positron production scales with Z_u^{18-20} where Z_u is the united charge of the collision system. Hence, below $Z_u \simeq 150$ nearly all measured positrons stem from nuclear transitions. In Fig. 8(a) examples of gamma spectra from these so-called "background systems" with $Z_u=137$ (U + Pd) and $Z_u=161$ (U + Tm) are given. (For the U + Tm system about 10% of the positrons originate from atomic

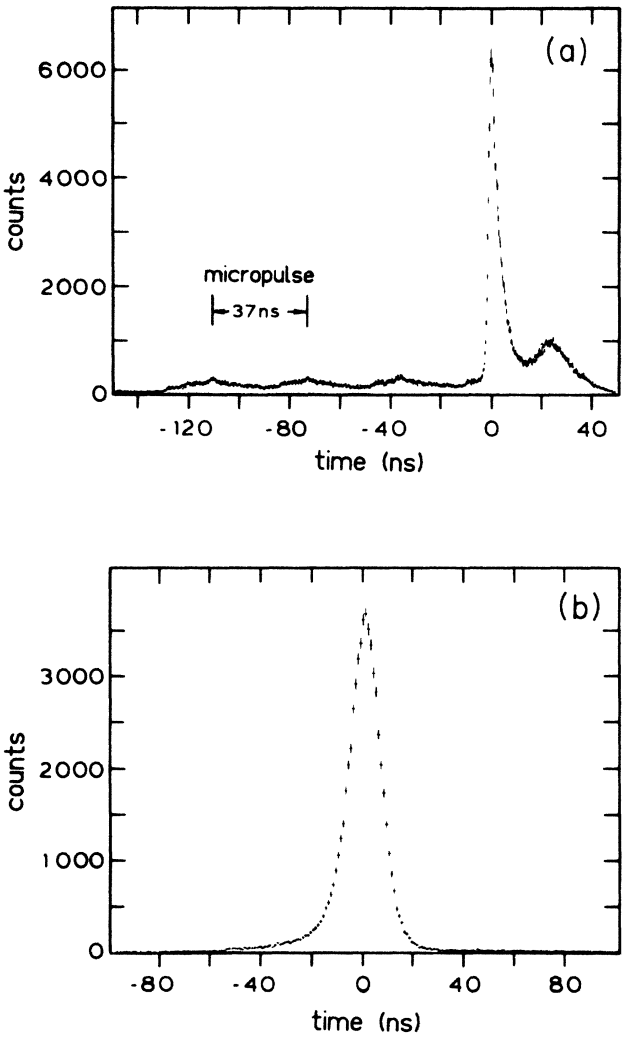

FIG. 5. Time difference between particle and gamma signals (a) and between one NaI segment and the positron-diode signal (b). The zero point is chosen arbitrarily.

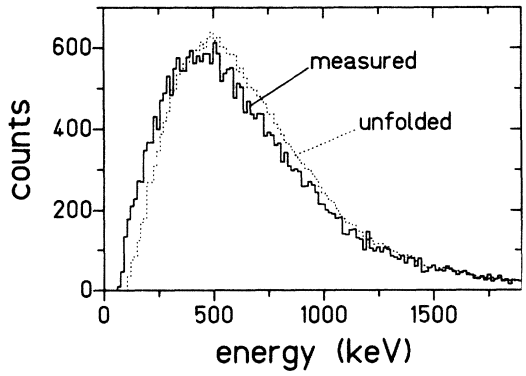

FIG. 6. Example of a raw and unfolded positron spectrum of the reaction U + U at 7.5 MeV/nucleon.

processes and this contribution has been taken into account in the analysis.) The positron spectra measured simultaneously and under the same kinematical conditions are presented in Fig. 8(b) together with the ones calculated from corresponding γ-ray spectra. The pair conversion coefficients $d\beta/dE_{e+}$ of Schlüter *et al.*[8] have been used.

All positron spectra coincident to elastic scattering can be reproduced assuming $E1$ transitions in the energy region above 1 MeV. These transitions originate from quasielastic processes which cannot be separated from pure elastic scattering by our particle counters. As shown in Fig. 8(b), the measured positron distribution meets the calculated one. Assuming the transition to be either in the projectile or in the recoil nucleus one obtains the two calculated curves which differ at low positron energies. As one expects, the experimental data lie in between. Since an $E1$ multipolarity is valid for a variety of collision systems at different kinematical conditions, the same multipolarity can be supposed for elastic collisions of U + U.

Dissipative collisions lead to high nuclear excitations. In analogy to (HI,xn) reactions, the γ spectra have been decomposed into a low-energy part with an exponential slope (collective $E2$ transitions) and a part reflecting statistical transitions. Figure 9 shows the spectral distributions of γ rays and positrons from dissipative U + Pd collisions at 8.4 MeV/nucleon. Assuming an $E1$ multipolarity for the high-energy transition the positron spectra (lower part of Fig. 9) can be reproduced by converting the measured γ spectra according to the ratio of the two contributions. Neither a single multipolarity ($E1$ yields too high and $E2$ too low calculated production probabilities), nor a simple mixture can reproduce the measured shape. The situation concerning the charge of the reaction products is simple because only the uranium fissions, yielding two Pd-like nuclei. As the outgoing products are the same in the dissipative U + U collisions, the same multipolarity can be supposed.

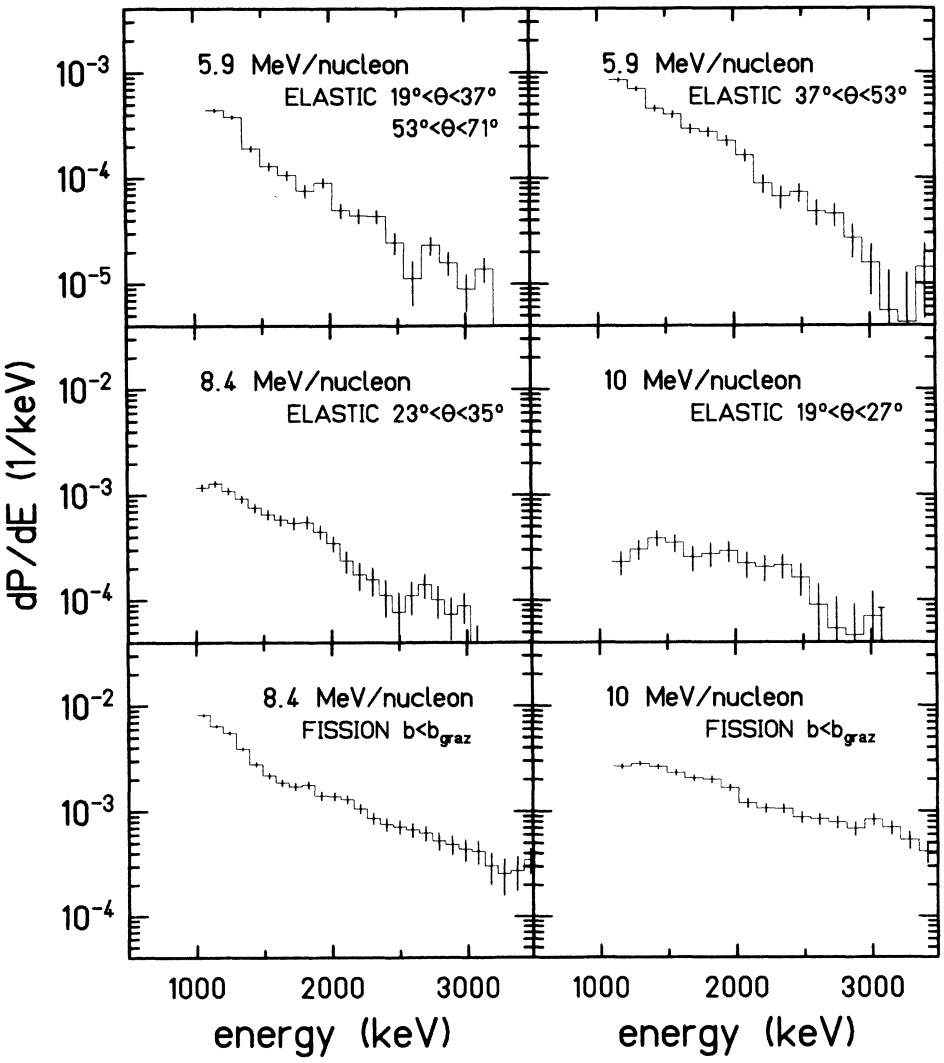

FIG. 7. Some unfolded γ-ray spectra above 1 MeV from U + U collisions.

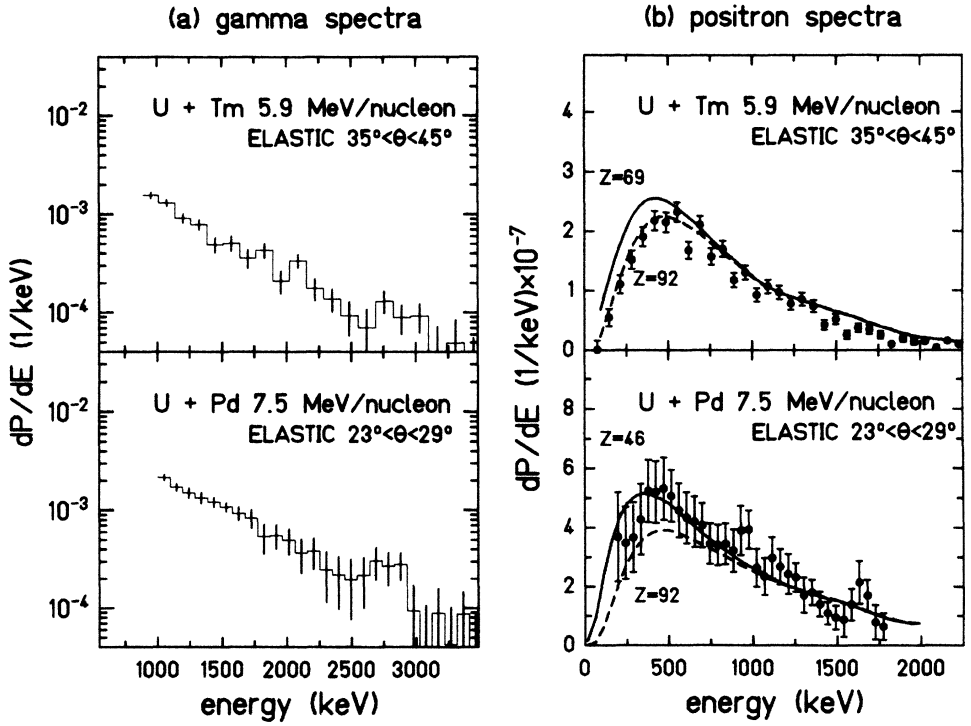

FIG. 8. (a) γ-ray spectra from collisions between uranium and lighter nuclei. (b) Positron spectra from the same reactions as shown in (a). The lines represent the spectra calculated with the noted charges and the multipolarities described in the text.

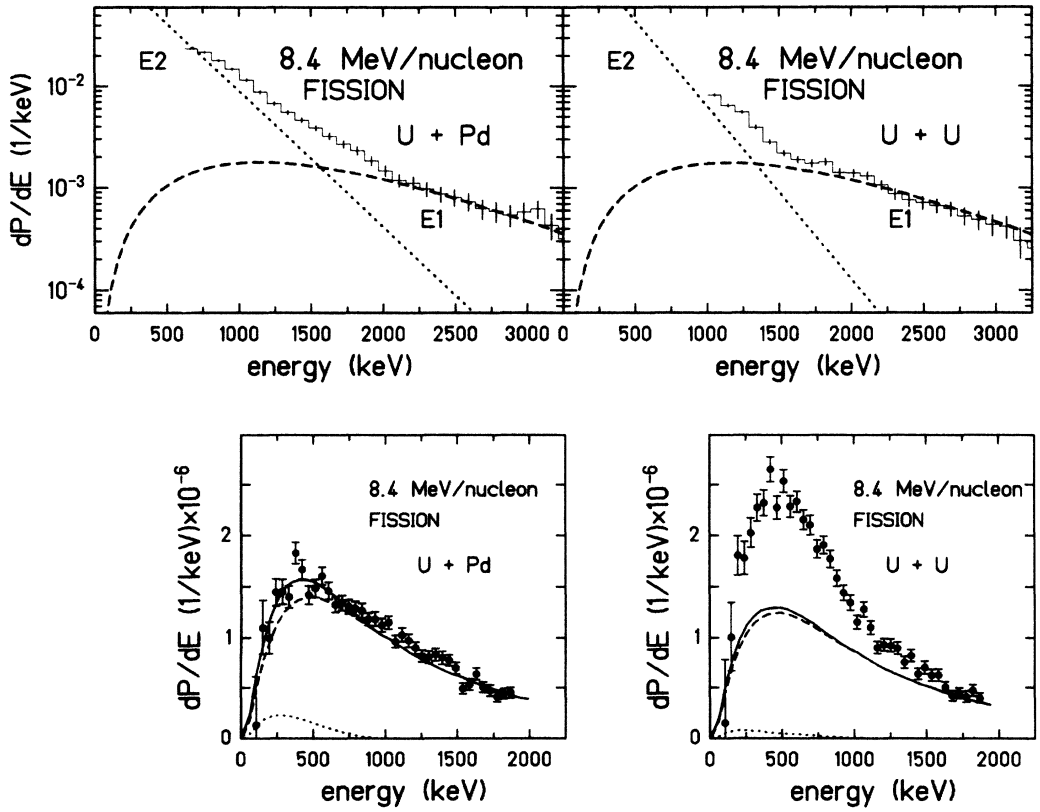

FIG. 9. Upper part: Decomposition of gamma spectra in an exponential part and one reflecting statistical transitions. Lower part: Corresponding contributions from $E1$ (dashed line) and from $E2$ (dotted line) to the calculated positron spectra (full line) from internal pair conversion.

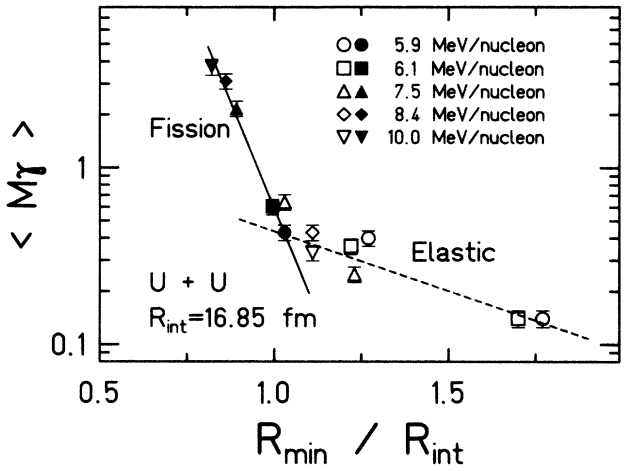

FIG. 10. Measured gamma-ray multiplicities for gamma energies above 1.2 MeV for uranium on uranium from 5.9 MeV/nucleon up to 10 MeV/nucleon as a function of the distance of closest approach. Elastic and dissipative collisions yield two different slopes.

One should note the importance of measuring gamma spectra with the same kinematical conditions as the positron spectra, since not only the contribution of different multipolarities can change, but also the average gamma multiplicity varies. The measured γ-ray multiplicities $\langle M_\gamma \rangle$ for gamma energy above 1.2 MeV is shown in Fig. 10 as a function of the distance of closest approach $R_{\min}$. Two different slopes can be seen corresponding to elastic scattering and dissipative collisions. This figure shows the consistency of our analysis. It is not straightforward to find a physical interpretation of these trends as $\langle M_\gamma \rangle$ does not contain γ rays below 1.2 MeV which essentially carry the angular momentum information. While nuclear excitations grow strongly with bombarding energy, it is interesting to note that the production probability for atomic positrons increases even faster. This is shown in Fig. 11 where the measured positron spectra and the calculated contributions from nuclear pair conversion are presented. The fraction of "nuclear" positrons decreases in relation to all positrons.

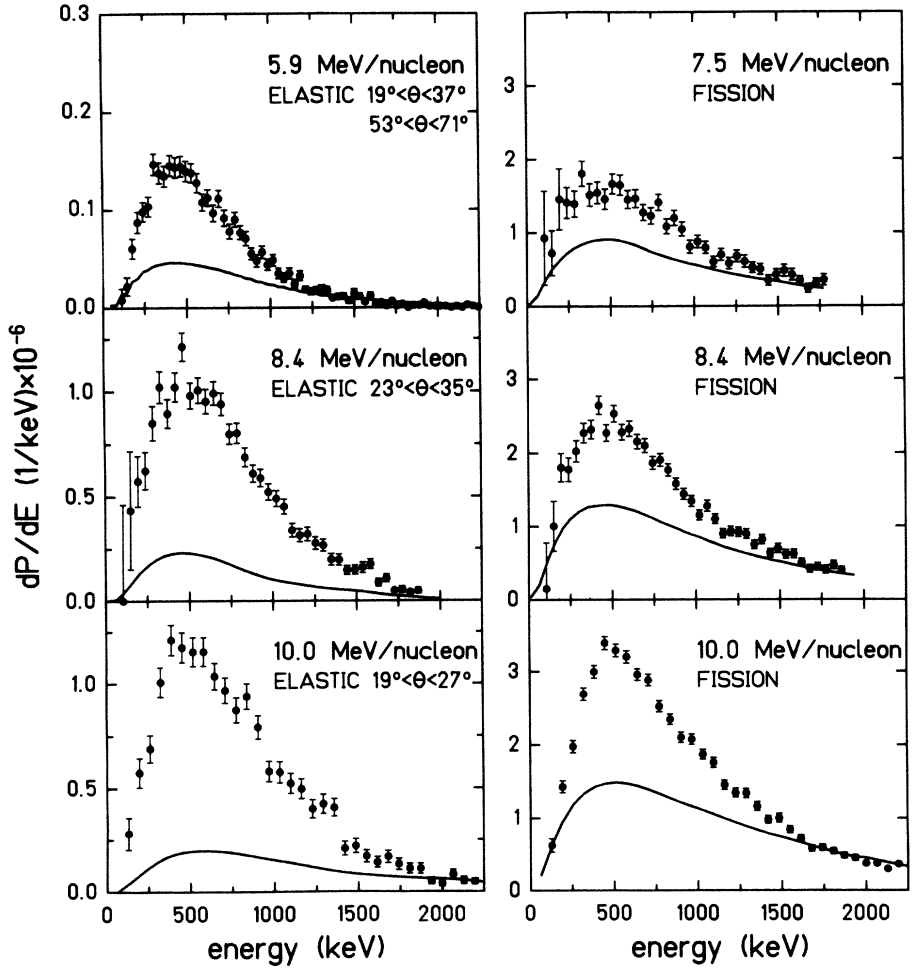

FIG. 11. Positron spectra from elastic and dissipative U + U collisions. The solid lines show the calculated contribution of positrons from nuclear origin. Note the different scales for dP/dE.

IV. RESULTS AND DISCUSSION

The collision system U + U was studied from the Coulomb barrier up to 10 MeV/nucleon incident energy. First we discuss electron and positron spectra associated with elastic scattering at various energies in order to test whether the total yield and energy distribution can be described in the framework of the above mentioned theoretical approaches assuming Rutherford trajectories. In Sec. IV B the same approach is applied to the positron and electron spectra measured in dissipative collisions using trajectories from different reaction models.

A. Positrons and electrons from elastic U + U collisions

In this subsection positrons and electrons emitted in elastic collisions from the Coulomb barrier up to 10 MeV/nucleon are discussed. Figure 12 shows positron spectra which mostly exhibit structureless shapes. These are well described by coupled-channels calculations[4] using Rutherford trajectories with normalization factors of 0.7—1.0. The analogous electron spectra (Fig. 13) are also well described by the same theoretical framework; however, normalization factors of 1.35 and 1.6 are needed. Note that the difference in production probability between positrons and electrons amounts to 4 orders of magnitude.

Figures 12(a) and 12(b) show atomic positron spectra from the U + U collision system at 5.9 MeV/nucleon incident energy, where only elastic scattering is expected. The spectral distribution of positrons from peripheral collisions (a) agrees well with the theory of dynamically induced (atomic) positrons normalized with a factor of 0.7. The slope of the electron spectrum [Fig. 13(a)] obtained under similar kinematical conditions also shows good

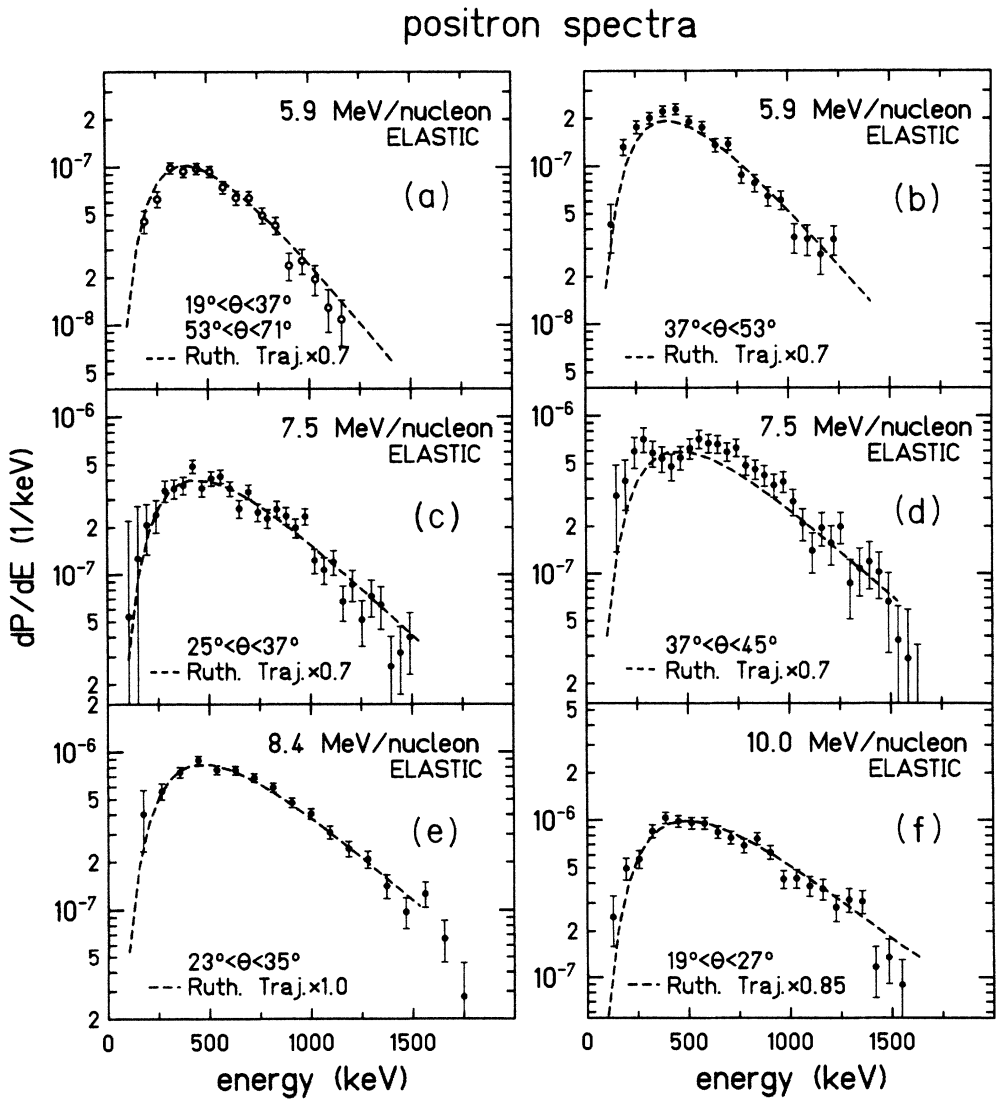

FIG. 12. Positron spectra from elastic U + U collisions at various incident energies.

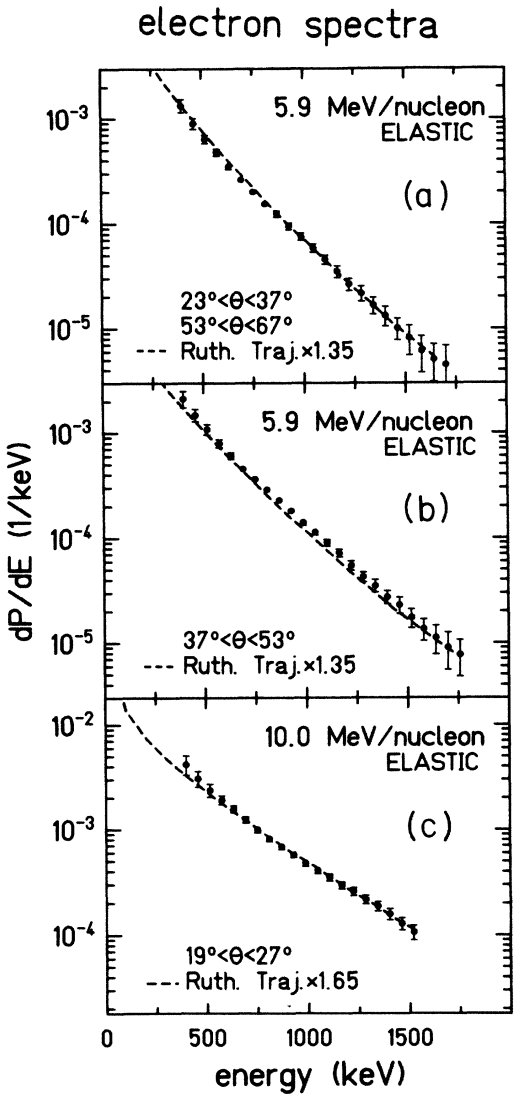

FIG. 13. Electron spectra from U + U collisions at 5.9 and 10.0 MeV/nucleon beam energy.

agreement with the coupled-channels calculations.[4]

The spectra in Figs. 12(b) and 13(b) represent the more central collisions (6.5 fm $< b <$ 11.5 fm). Compared with theoretical calculations scaled with the same factors as above, the positron spectrum shows an enhancement of 20% around 300 keV. This might be correlated with the observation of peak structures reported elsewhere.[9] Lineshape structures in positron spectra around 320 keV have been observed in heavy collision systems at the Coulomb barrier. These structures have attracted a lot of interest but are unexplained up to now. In a different experiment oriented to this point we observed peak-like structures when requiring special kinematical conditions. They appear less pronounced than reported in Ref. 9. These results will be the subject of a forthcoming paper.

The experimental points for electrons around 1 MeV lie above the theoretical line [Fig. 13(b)]. This enhancement is not understood and could arise from nuclear transitions via conversion processes in ^{238}U. The corresponding γ spectra (see Fig. 7) show no significant enhancement, therefore suggesting $E0$ transitions.

At 7.5 MeV/nucleon the positron spectra are presented for two impact parameter regimes defined by the laboratory scattering angles $25° < \theta < 37°$ and $37° < \theta < 45°$. The experimental points measured close to the grazing angle deviate from a smooth distribution showing an unexpected bumplike structure. Quasielastic processes might be the origin.

The positron spectra obtained at 8.4 MeV/nucleon and 10 MeV/nucleon shown in Figs. 12(e) and 12(f), respectively, exhibit smooth curves which agree well with the theory. The γ-electron spectrum measured at 10 MeV/nucleon under the same kinematical condition as positrons is shown in Fig. 13(c). To describe the data the theoretical values have to be multiplied by a factor 1.6.

In summary, positrons and electrons emitted in elastic collisions are well described in shape by theory; the calculated intensities have to be decreased for positrons ($\simeq$0.8) and increased for electrons ($\simeq$1.5). Some spectra obtained under selected kinematical conditions show an unexplained enhancement.

B. Positrons and electrons associated with dissipative collisions

Positron spectra from dissipative U + U collisions were measured at 7.5, 8.4, and 10 MeV/nucleon and at the latter energy δ-electron distributions were also obtained.

Dissipative collisions in the U + U system are well distinguished from elastic and quasielastic processes since at least one and usually both reaction products fission. This property of the U + U system leads to a broad distribution of the outgoing fragments in the angular correlation plane as shown in Fig. 14(a). By our counter positioning we detect an unbiased ensemble from all impact parameters as verified by Monte Carlo calculations.

In Sec. IV B 2 selected subclasses of dissipative collisions are discussed. The identified three- and four-body events [Figs. 14(b) and 14(c)] reflect different impact-parameter regimes.

In the theoretical calculations the trajectory of a binary system is considered, which implies that fission does not modify the electron emission in the observed energy range. This assumption is justified by measurements[10] showing that fission occurs when the two nuclei are separated by at least 100 fm. However, at higher energies this is not necessarily true and a fast breakup could happen. Such a process would yield very different positron and electron spectra.[4]

1. Nuclear contact times and test of reaction models

The electron spectra obtained in coincidence with two different reaction mechanisms are shown in Fig. 15. The upper part again shows the data from elastic scattering exhibiting good agreement with the calculation. Electrons originating from dissipative collisions (lower part) exhibit

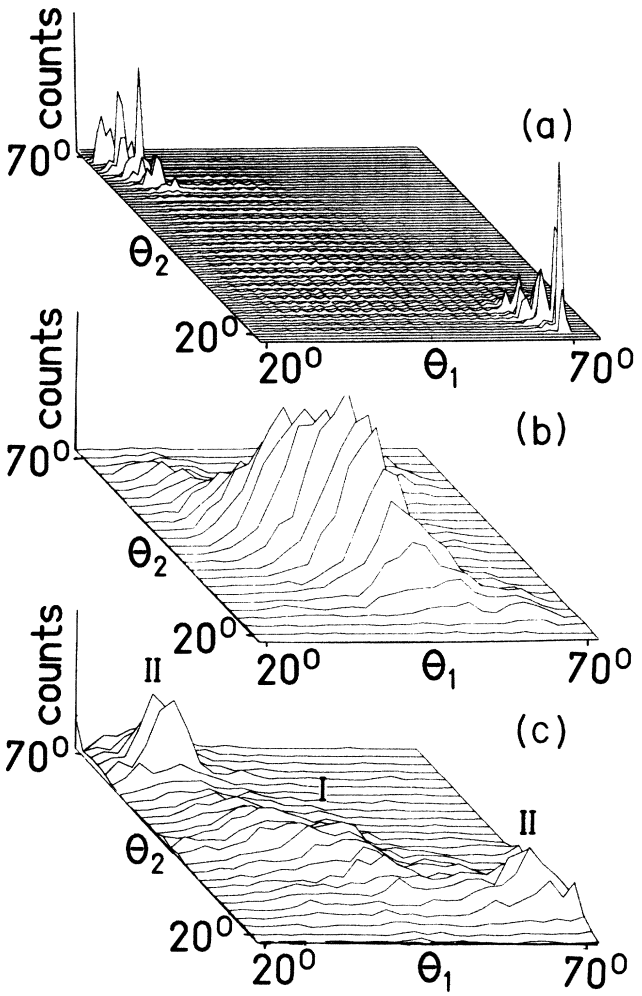

FIG. 14. θ_1-θ_2 correlation between the emitted fragments in the collision U + U at 10.0 MeV/nucleon. (a) All events exhibiting two classes: elastic scattering with $\theta_1+\theta_2=90°$ and sequential fission observed by their broad distribution. (b) Only identified four-body events. (The given angles refer to the average of the measured angles.) (c) Only identified three-body events. For (b) and (c) see text Sec. IV B 2.

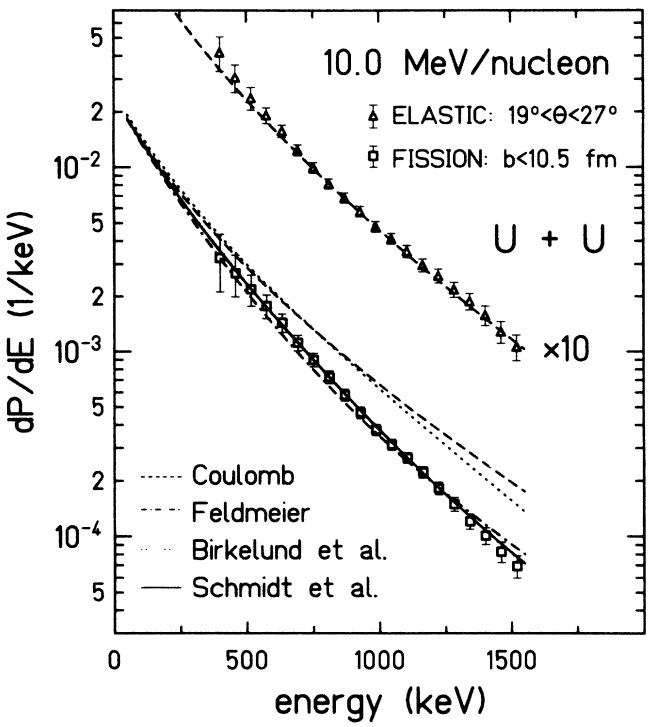

FIG. 15. Electron spectra from elastic scattering and fission reactions compared with scaling-model (Ref. 2) calculations based on different reaction models.

a steeper slope than expected for elastic processes. Their shapes cannot be reproduced using Rutherford trajectories. One has to adopt trajectories determined from a reaction model which is adequate for deep inelastic processes. Among many different models of deep inelastic reactions three were chosen to calculate trajectories.

The two macroscopic friction models use classical equations of motion and a Coulomb and proximity potential. In the one proposed by Birkelund *et al.*,[11] the friction coefficients, which are the essential quantity, are fitted mainly to fusion reactions where heavy-on-heavy systems are hardly considered. Schmidt *et al.*[12] apply a dominant radial friction factor which leads to a fast deceleration when the two nuclei approach. This can be seen from Fig. 16 which shows the interaction distance as a function of time for the various models. Schmidt *et al.* only simulate the neck formation to yield the Q values as measured in damped collisions while Feldmeier[13] treats the deformation of the nuclei in detail. In Feldmeier's model the motion of the nuclear matter follows a Langevin equation with collective degrees of freedom describing the shape of the system. It should be mentioned that this model includes a fluctuation force, but for the calculations used in this paper only the mean trajectories are taken.[14] The latter model leads to a smoother trajectory than the one of Schmidt *et al.* In both models the trajectories strongly deviate from Coulombic ones and significant nuclear interaction times result. The definition of the quantity t_{int} can be seen from Fig. 1 and the values obtained by these models are given in Fig. 17 as a function of the impact parameter.

One should remember that the parametrization of $\dot{R}/R$ implies an interaction time defined by the maxima of the $\dot{R}/R$ curve. In the perturbation model[2] it is assumed that the distance R does not vary during this time. In this respect, the trajectories of Schmidt *et al.* are best suited for the calculation. Our definition still yields well-defined interaction times, e.g., for the realistic trajectories of Feldmeier. It turns out that t_{int} indeed reflects the time of nuclear interactions, as the maxima of $\dot{R}/R$ in the outgoing trajectory occur just at the instant when the trajectories become Coulombic.

The results of these calculations are compared in Fig. 15 with the experimental data. The slope of the measured production probability as a function of the electron energy

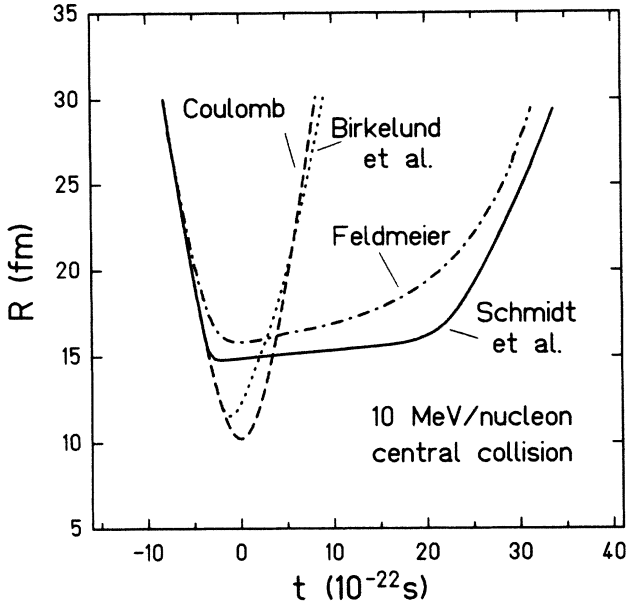

FIG. 16. Time dependence of the internuclear distance according to various reaction models.

is well reproduced by the two friction models of Schmidt *et al.* and of Feldmeier. The interaction times are about 2×10^{-21} s for the most central collisions (see Fig. 17). Since there is no significant difference between the calculated results, the positron spectra are analyzed in the framework of the Schmidt model only.

The shape of positron spectra associated with deep inelastic collisions of U + U at all studied bombarding energies are in good agreement with theoretical results based on the friction model of Schmidt *et al.* (Fig. 18). Multi-

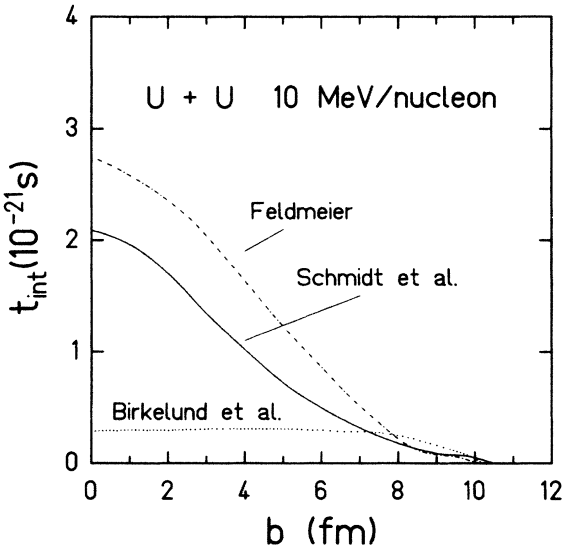

FIG. 17. Nuclear interaction times vs impact parameter calculated from the various reaction models.

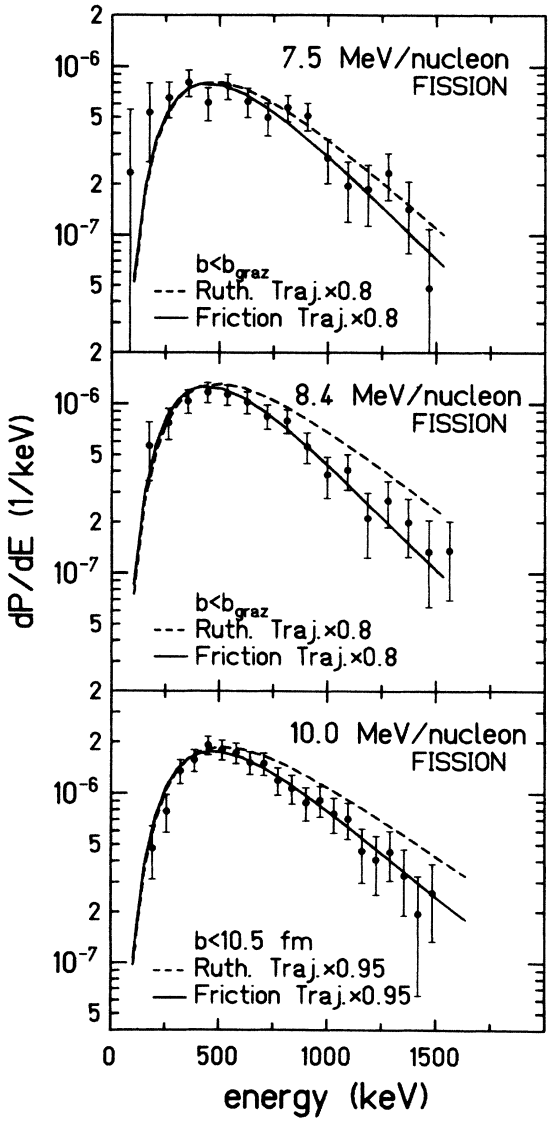

FIG. 18. Comparison of measured and calculated positron spectra for dissipative collisions at 7.5, 8.4, and 10.0 MeV/nucleon.

plication factors of 0.8, 0.8, and 0.95 for the incident energies 7.5, 8.4, and 10 MeV/nucleon, respectively, are used while the calculated electron spectra have to be normalized with 1.6 to fit the data as it was found studying elastic collisions. The predictions based on Rutherford trajectories differ significantly as it was found for δ electrons. This model yields nuclear interaction times up to 1.2×10^{-21} s, 1.7×10^{-21} s, and 2.1×10^{-21} s for dissipative reactions at 7.5, 8.4, and 10 MeV/nucleon, respectively.

The normalization factors between theory and the experimental result show the same trend as already found for elastic scattering. At present it is not understood why the theory slightly overestimates positron and underestimates δ-electron production probability. To a small ex-

tent the variation of the normalization factors could result from errors in the efficiency determination (error ±5%), as there were two experimental series (one at 5.9 and 10.0 MeV/nucleon and the other at 7.5 and 8.4 MeV/nucleon). Possible errors in determining the contributions from nuclear transitions alone cannot explain the variation. Both for the positron and electron production a clear trend can be seen showing normalization factors increasing with bombarding energy.

A different method to study nuclear contact times in U + U collisions at 7.5 MeV/nucleon incident energy was used by Stoller *et al.*[15] In their analysis they considered only the very rare events with Q values up to -200 MeV that still yielded two U-like stable nuclei. From the corresponding K-shell ionization probability, nuclear reaction times of about 1×10^{-21} s were extracted.

Nuclear contact times can also be extracted using simple classical assumptions to deduce the deflection function from the experimental cross sections $d^2\sigma/dE\,d\theta$. In Ref. 16 this method is applied to the results of the reaction U + U at 7.42 MeV/u (Ref. 17). This model-dependent procedure has been studied in detail also in Ref. 18 and yields nuclear contact times up to 5×10^{-21} s.

2. *Positrons from subgroups of dissipative collisions*

While in the previous chapter all dissipative collisions are studied in total, we will now discuss subgroups of identified three- and four-body events which may be ascribed to selected ranges of impact parameter. As mentioned in the introduction, the selection of impact parameter regimes allows a more detailed study of dissipative reactions via electron and positron spectroscopy.

Due to the double readout of the PPAC it is possible to detect both fission fragments in a single counter. Figure 14(b) shows the subgroup of four-body events, where each PPAC has detected two fragments. The average of the two angles in one counter is presented which corresponds roughly to the primary scattering angle of the fissioning nucleus. The large opening of the fission cone leads to a decreasing detection efficiency towards the edges of the counters. Therefore mainly events with primary angles around 45° are detected. In many cases one fragment misses a counter and could be misinterpreted as a three-body event. To distinguish these from true three-body events a ΔE signal characterizing U-like nuclei is required in the counter with one hit. The class of true three-body events is shown in Fig. 14(c). Two distinct groups can be seen: (i) collisions with high Q values and laboratory scattering angles around 30°–50°, and (ii) collisions with low energy loss and scattering angles close to the grazing angle.

From the angular correlation Q values have been calculated neglecting mass transfer and geometrical effects (see below) and are shown in Fig. 19. The distribution corresponding to three-body events contrasts with the Gaussian shape of four-body events. The mean energy loss of class (i) is even higher than that of four-body fission. The two classes of three-body events can be explained as there are two possibilities for uraniumlike nuclei to survive: (i) A large mass transfer yields one "light" fragment ($Z<82$) which hardly fissions. This process happens for high Q values. (ii) In peripheral collisions the nuclei are excited much less.

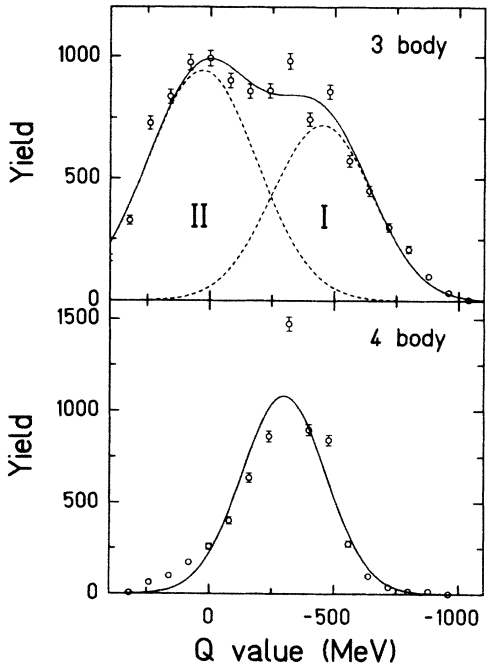

FIG. 19. Q-value distributions of three- and four-body events.

The Q values in Fig. 19 are determined under the assumption that the average between the two polar angles yields the primary scattering angle as mentioned. In order to estimate systematic errors and the precision of this procedure a Monte Carlo program was developed to simulate sequential fission. For the primary reaction, impact-

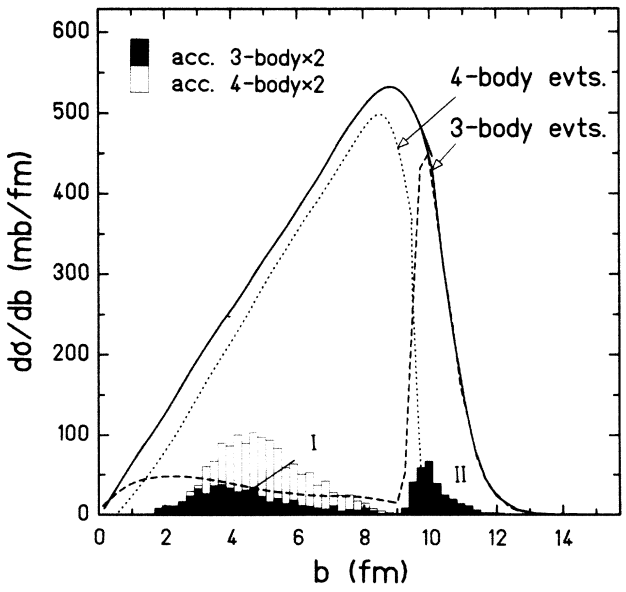

FIG. 20. Impact parameter distributions of various dissipative processes (dashed and dotted lines) and the fraction detected by the particle counters (histograms).

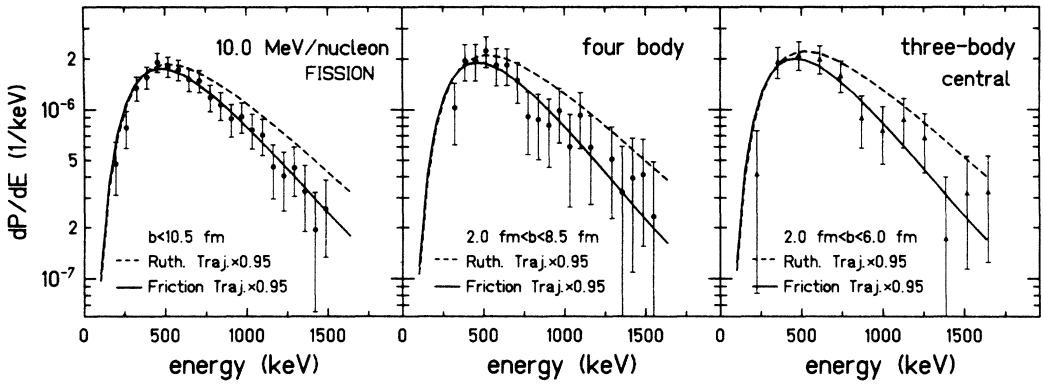

FIG. 21. Comparison of positron spectra associated with different impact parameter regimes.

parameter-dependent Q values[12] and a deflection function proposed by Schmidt *et al.*[12] and a fixed mass distribution extrapolated from Ref. 17 were used. The sequential fission is calculated using total kinetic energy (TKE) values from the Viola systematics[19] and fission fragment mass distributions suggested by Ref. 20. The width of the mass distribution affects the results very little. Using these Monte Carlo simulations the Q values presented in Fig. 19 have been corrected and a mean Q value of four-body events of -395 MeV with an error of ± 70 MeV is obtained. The two classes of three-body reactions correspond to Q values of -50 and -450 MeV, respectively, with an error of ± 70 MeV.

In a second step we study the repartition into three- and four-body events. Using a deflection function[12] in these calculations, impact parameter regimes leading to the various processes are obtained. The dotted and dashed lines in Fig. 20 represent the distributions of three- and four-body reactions. Their shapes are adjusted to fit the measured θ_1-θ_2 distribution shown in Fig. 14. The histograms in Fig. 20 represent the fraction of events detected by the counters. Again, the two classes of three-body events are seen: peripheral (ii) and central (i) collisions.

In Fig. 21 the measured positron spectra corresponding to all dissipative collisions, to identified four-body and to class (i) three-body events, are compared with coupled-channels calculations which are based on the impact parameter selection given in Fig. 20. The calculated slopes become only slightly steeper when choosing more and more central collisions. Within the limited statistics the data agree with the theory. Very clearly the absolute yield increases by 10% from all reactions to the four-body events and again by 20% from four-body to three-body central-collision events. This agrees with the theory and proves that more and more central collisions are selected.

As mentioned in the introduction oscillations in the spectra are observable if the range of interaction time is sufficiently narrow. As impact parameters and interaction time are correlated (see Fig. 17) the presented selection is a promising step towards the observation of fluctuations. The limited statistics do not allow for a finer analysis, e.g., further restriction of the impact parameter range via additional Q-value cuts. This possibility will be investigated extensively in future experiments.

V. CONCLUSIONS

Elastic scattering and dissipative collisions of U + U were studied at various incident energies from the Coulomb barrier (5.9 MeV/nucleon) up to 10 MeV/nucleon. Both the positron and the electron spectra associated with the two mechanisms show significant differences. The spectra are compared with theory using Rutherford trajectories and trajectories from models for deep inelastic collisions. The main results are as follows:

(i) Measured positron and δ-electron spectra associated with elastic collisions of the U + U system up to 10 MeV/nucleon are well reproduced by the theory assuming pure Rutherford trajectories. Positrons emitted under selected kinematical conditions at bombarding energies 5.9 and 7.5 MeV/nucleon exhibit an approximately 20% enhancement for positrons and electrons of certain energies. This observation might be correlated with the measured line structures reported elsewhere.[9]

(ii) The positron and δ-electron spectra obtained in coincidence with dissipative collisions exhibit much steeper slopes in the measured energy range than expected from calculations based on Rutherford trajectories. This effect can be explained assuming contact times up to 2×10^{-21} s. Positron and δ-electron spectra give a new possibility to test reaction models. This is demonstrated by one measured δ-electron spectrum which is compared to calculations using trajectories from three different friction models. The shape is reproduced best by the models of Schmidt *et al.*[12] and of Feldmeier.[13]

Subgroups of the dissipative collisions had been separated via the division into three- and four-body events. The associated positron spectra show that different ranges of impact parameters are selected. The tech-

nique of impact parameter selection gives hope to observe in future experiments the oscillations which allow a model-independent determination of nuclear contact times.

(iii) The shape of the positron and electron data both for elastic and dissipative collisions are well described by coupled-channels calculations. Their absolute yields have to be normalized by factors ranging from 0.7 to 1.0 for positrons while the electron emission is underestimated requiring normalization factors of 1.35–1.6.

ACKNOWLEDGMENTS

We would like to acknowledge U. Müller, T. de Reus, and G. Soff for performing the coupled-channels calculations and for many very fruitful discussions. We would like to thank J. Foh, Institut für Kernphysik, for building dedicated electronics, and H. Folger and the GSI target laboratory for the preparation of the excellent targets. This work was supported by the Bundesministerium für Forschung und Technology and by the Gesellschaft für Schwerionenforschung, Darmstadt.

---

*On leave from Institut of Nuclear Physics, Cracow, Poland.

†Present address: University of Mainz, Federal Republic of Germany.

[1]B. Müller, J. Rafelski, and W. Greiner, Z. Phys. **257**, 62 (1972); **257**, 183 (1972); J. Reinhardt and W. Greiner, Rep. Prog. Phys. **40**, 219 (1977).

[2]E. Kankeleit, Nukleonika **25**, 253 (1980).

[3]H. Backe, P. Senger, W. Bonin, E. Kankeleit, M. Krämer, R. Krieg, V. Metag, N. Trautmann, and J. Wilhelmy, Phys. Rev. Lett. **50**, 1838 (1983).

[4]G. Soff, J. Reinhardt, B. Müller, and W. Greiner, Phys. Rev. Lett. **43**, 1981 (1979); T. de Reus, J. Reinhardt, B. Müller, W. Greiner, G. Soff, and U. Müller, J. Phys. B **17**, 615 (1984); U. Müller, G. Soff, J. Reinhardt, T. de Reus, B. Müller, and W. Greiner, Phys. Rev. C **30**, 1199 (1984); T. de Reus, J. Reinhardt, B. Müller, W. Greiner, U. Müller, and G. Soff, *Progress in Particle and Nuclear Physics,* edited by A. Faessler (Pergamon, New York, 1985), Vol. 15, p. 57.

[5]E. Kankeleit, U. Gollerthan, G. Klotz, M. Kollatz, M. Krämer, R. Krieg, U. Meyer, H. Oeschler, and P. Senger, Nucl. Instrum. Methods A **234**, 81 (1985).

[6]M. Krämer, Diplomarbeit, Technische Hochschule Darmstadt, 1982.

[7]H. Backe, W. Bonin, E. Kankeleit, M. Krämer, R. Krieg, V. Metag, P. Senger, N. Trautmann, F. Weik, and J. Wilhelmy, in *QED of Strong Fields,* Nato Advanced Study Institute Series B, edited by W. Greiner (Plenum, New York, 1983), p. 107.

[8]P. Schlüter, G. Soff, and W. Greiner, Phys. Rep. **75**, 327 (1981).

[9]J. Schweppe, A. Gruppe, K. Bethge, H. Bokemeyer, T. Cowan, H. Folger, J. Greenberg, H. Grein, S. Ito, R. Schulé, D. Schwalm, K. E. Stiebing, N. Trautmann, P. Vincent, and M. Waldschmidt, Phys. Rev. Lett. **51**, 2261 (1983); M. Clemente, E. Berdermann, P. Kienle, H. Tsertos, W. Wagner, C. Kozhuharov, F. Bosch, W. König, Phys. Lett. **137B**, 41 (1984); T. Cowan, H. Backe, M. Begemann, K. Bethge, H. Bokemeyer, H. Folger, J. S. Greenberg, H. Grein, A. Gruppe, Y. Kido, M. Klüver, D. Schwalm, J. Schweppe, K. E. Stiebing, N. Trautmann, and P. Vincent, Phys. Rev. Lett. **54**, 1761 (1985); H. Tsertos, E. Berdermann, F. Bosch, M. Clemente, P. Kienle, W. König, C. Kozhuharov, and W. Wagner, Phys. Lett. **162B**, 273 (1985).

[10]P. Glässel, D. v. Harrach, H. J. Specht, and L. Grodzins, Z. Phys. A **310**, 189 (1983).

[11]J. Birkelund, L. Tubbs, J. Hui, J. De, and D. Sperber, Phys. Rep. **56**, 107 (1979).

[12]R. Schmidt, V. Toneev, G. Wolschin, Nucl. Phys. **A311**, 247 (1978).

[13]H. Feldmeier, in *Nuclear Structure and Heavy-Ion Dynamics,* Course LXXXVII, Societá Italiana di Fisica, Bologna, edited by L. Moretto and R. Ricci (North-Holland, Amsterdam, 1984). In this model the distance R is calculated via the rms charge distribution of two penetrating nuclei.

[14]E. Kankeleit, in Gross Properties of Nuclei and Nuclear Excitations, International Workshop XIII, Hirschegg, Austria, January, 1985, edited by H. Feldmeier.

[15]Ch. Stoller, M. Nessi, E. Morenzoni, W. Wölfli, W. E. Meyerhof, J. D. Molitoris, E. Grosse, and Ch. Michel, Phys. Rev. Lett. **53**, 1329 (1984).

[16]G. Wolschin, Nukleonika **22**, 1165 (1977).

[17]H. Freisleben, K. D. Hildenbrand, F. Pühlhofer, W. F. Schneider, R. Bock, D. v. Harrach, and H. J. Specht, Z. Phys. A **292**, 171 (1979).

[18]R. Krieg, Ph.D. thesis, Technische Hochschule Darmstadt, 1985.

[19]V. E. Viola, Jr., Nucl. Data A **1**, 391 (1966).

[20]R. Vandenbosch and J. R. Huizenga, *Nuclear Fission* (Academic, New York, 1973).